

Diversity of structural phases and resulting control of properties in brownmillerite oxides: A first-principles study

Hao Tian,^{1,2,3} L. Bellaïche,³ and Yurong Yang^{1,2,3,*}

¹National Laboratory of Solid State Microstructures and Collaborative Innovation Center of Advanced Microstructures, Department of Materials Science and Engineering, Nanjing University, Nanjing 210093, China

²Jiangsu Key Laboratory of Artificial Functional Materials, Nanjing University, Nanjing 210093, China

³Physics Department and Institute for Nanoscience and Engineering, University of Arkansas, Fayetteville, Arkansas 72701, USA



(Received 7 June 2019; revised manuscript received 27 September 2019; published 26 December 2019)

First-principles calculations are conducted on a prototype of brownmillerite oxides, that is, $\text{Ca}_2\text{FeAlO}_5$, to explain and reveal the existence of many structural states, including ones with long periods, having close energy but rather different physical properties. Examples are polar states with different quantized-like electrical polarizations and significant linear magnetoelectric coefficients, as well as antipolar phases. These states can also differentiate themselves by the direction of their predominant antiferromagnetic vector and of their weak magnetization, which hint towards unusual magnetoelectric effects such as rotating the magnetization by applying an electric field. All these features can be traced back to the oxygen tetrahedral pattern that is inherent to brownmillerites, and the energetic easiness to alter such pattern. Furthermore, these features are also found in other brownmillerites, which emphasizes the generality.

DOI: [10.1103/PhysRevB.100.220103](https://doi.org/10.1103/PhysRevB.100.220103)

The class of $A_2B_2O_5$ brownmillerites, that can be thought as resulting from the introduction of oxygen vacancies in the ABO_3 perovskite structure, is known to exhibit diverse and rich properties (note that oxygen vacancies are neutral in brownmillerites, which can contrast with the case of defects in perovskites, such as BiFeO_3 [1]). Examples include ferro-magnetism, antiferromagnetism, magnetic frustration, metal-insulator transitions, colossal magnetoresistance, and different spin and orbital orderings [2–4]. Brownmillerites can play a significant role for various technological applications, such as energy conversion, catalysts, sensors, solid oxide fuel cells, etc. [5–8].

Strikingly, many structural phases, with rather different properties, have been reported in various brownmillerite compounds, as shown in Table SI of the Supplemental Material [9]. For instance, $\text{Sr}_2\text{CoFeO}_5$ [10] and $\text{Sr}_2\text{MnGeO}_5$ [11] display the high-symmetry paraelectric $Imma$ structure at ambient conditions. In contrast, $\text{Ca}_2\text{Fe}_2\text{O}_5$ and $\text{Ca}_2\text{FeGaO}_5$ adopt the antipolar $Pnma$ symmetry, while $\text{Ba}_2\text{InGaO}_5$ [12] has a polar $Ima2$ space group symmetry. A more complex (paraelectric) $Pbcm$ state with doubling of the unit cell along the c axis was even recently observed at room temperature in $\text{Ca}_2\text{Co}_2\text{O}_5$ and $\text{Ca}_2\text{FeCoO}_5$ [13,14]. Furthermore, with decreasing temperature, $\text{Ca}_2\text{Co}_2\text{O}_5$ undergoes a reentrant sequence of the following first-order structural phase transitions: $Pcmb-P2/c11-P12_1/m1-Pcmb$. Note also that several conflicting phases have been suggested for $\text{Sr}_2\text{Co}_2\text{O}_5$, namely, $Imma$, $Ima2$, and $Pnma$ [15,16]. These diverse symmetries of phases in $A_2B_2O_5$ brownmillerites have the potential to result

in various electronic, electrical, magnetic, and magnetoelectric properties.

One may wonder if there is a microscopic feature that is responsible for the diversity of such phases, and if such hypothetical feature can even result in other low-energy phases that are not yet known but also in precise control of physical properties in brownmillerites. The goal of this Rapid Communication is to demonstrate that this is indeed the case. More precisely, the microscopic feature is the relative energetic easiness of modifying the pattern of oxygen tetrahedral tiltings of brownmillerites [as shown in Fig. 1(a), the $A_2B_2O_5$ brownmillerite structure consists of sheets of apex-linked BO_6 octahedra interlinked with sheets of BO_4 tetrahedral coordination sites]. Furthermore, this modification results in, e.g., (1) long-period and presently unknown structural phases; (2) quantification of electrical polarization in some polar states; (3) rotating the easy magnetic axis (of the antiferromagnetic vector) and the magnetization direction; and (4) potentially inducing significant and/or unusual magnetoelectric effects. This work therefore not only successfully explains the diversity in symmetry of brownmillerite structures but also can open a new avenue to design, e.g., novel ferroelectrics, antiferroelectrics, and multiferroics.

To reveal such striking features, we focused on the classical brownmillerite $\text{Ca}_2\text{FeAlO}_5$, which is a naturally occurring mineral form that has been known for more than five decades [17], and conducted *ab initio* simulations on it. As indicated in the Supplemental Material (see Fig. S1 and Table SII), we considered different types of chemical ordering between Al and Fe ions for $\text{Ca}_2\text{FeAlO}_5$ brownmillerites, and numerically found that the ordering for which Al ions are located at the oxygen tetrahedra layers while the Fe ions are at the center of the oxygen octahedra provides the lowest total energy

*yangyr@nju.edu.cn

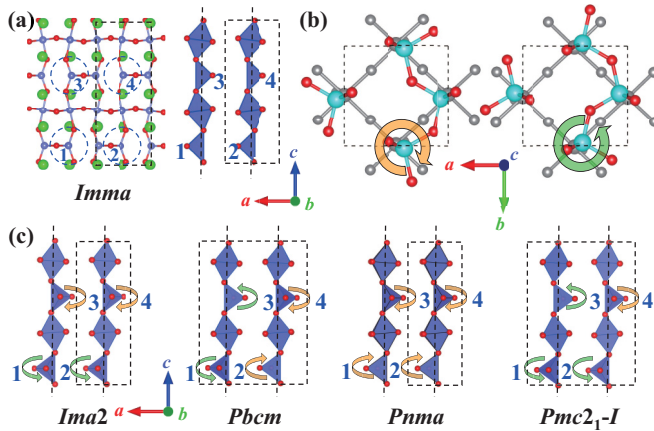


FIG. 1. Different phases, and some of their characteristics, in brownmillerites. Panel (a) displays the high-symmetry *Imma* phase and its polyhedral pattern, with four different types of oxygen tetrahedra (denoted as “1”, “2”, “3”, and “4”). Panel (b) shows the possible tilting of the tetrahedron of type “3” or “4”, that is clockwise (in orange) versus counterclockwise (in green), which induces an electric dipole being oriented along \mathbf{b} versus $-\mathbf{b}$, respectively. Panel (c) depicts the tilting pattern for the *Ima2*, *Pnma*, *Pbcm*, and *Pmc2₁-I* phases, with the tetrahedra of types “1”, “2”, “3”, and “4” being indicated there too.

among the investigated ones [see Fig. 1(a) for the locations of oxygen octahedra layers and tetrahedra layers within the brownmillerite structure]. Such finding is consistent with the experimental observation that the centers of the oxygen octahedra are in majority occupied by Fe ions (namely, 75% of the Fe ions are located at such centers [18,19]). Consequently, we focus here on this specific chemical ordering, and performed density functional theory (DFT) calculations [20], as detailed in the Supplemental Material [21–29].

Let us start by investigating, in $\text{Ca}_2\text{FeAlO}_5$, the five structures that were found to have low energy for $\text{Sr}_2\text{Co}_2\text{O}_5$ brownmillerites in Ref. [30]. They are the high-symmetry *Imma* structure (that has 36 atoms in its unit cell), and the following four phases that mostly differentiate themselves from the pattern, along the z axis, of the rotation of the four types of oxygen tetrahedra denoted as “1”, “2”, “3”, and “4” in Fig. 1(a) [note that if one takes the center of tetrahedron “1” of Fig. 1(a) to be at the origin of the coordinates, then tetrahedra “2”, “3”, and “4” have centers located at about $\mathbf{a}/2$, $\mathbf{c}/2$, and $(\mathbf{a} + \mathbf{c})/2$, respectively, where \mathbf{a} and \mathbf{c} are two lattice vectors of the *Imma* structure]: *Ima2*, that has 36 atoms per unit cell and a “mm/pp” tilting pattern, where “p” and “m” refer to a positive (clockwise) and negative (counterclockwise) rotation, respectively, with respect to the trigonometric direction of rotation, and where the two letters on the left side of the “/” symbol characterize the tilting of the tetrahedra of types “1” and “2” within a (001) plane, respectively, while the two letters on the right side of the “/” symbol represent the tilting of the tetrahedra of types “3” and “4” within another (001) plane, respectively; *Pnma*, that also has 36 atoms per cell but possesses a “pp/pp” tilting pattern; *Pbcm*, that has 72 atoms per unit cell and exhibits an “mp/mp” tilting pattern; and *Pmc2₁-I*, that also has 72 atoms in its unit cell but is characterized by an “mm/mp” tilting pattern. Note that we

use the notation *Pmc2₁-I* because other phases having the same space group of *Pmc2₁* will be discussed later on. It is also worthwhile to realize that, as shown in Table SI of the Supplemental Material [9], *Imma*, *Pnma*, *Ima2*, and *Pbcm* have been observed in various brownmillerites, while *Pmc2₁-I* was recently predicted to be the ground state for $\text{Sr}_2\text{Co}_2\text{O}_5$ [30]. Interestingly, out of these five phases, “only” *Ima2* and *Pmc2₁-I* can adopt a spontaneous electrical polarization. We will later explain such fact.

Note also that we considered different spin orders, namely, ferromagnetic (FM), A-type antiferromagnetic, C-type antiferromagnetic, and G-type antiferromagnetic (G-AFM) for the Fe cations, and found that this latter magnetic arrangement is preferred for all the aforementioned five phases in $\text{Ca}_2\text{FeAlO}_5$ (see Table SIII of the Supplemental Material [9]). We will thus from now on only concentrate on G-AFM ordering.

Table I reports the total energy of the relaxed *Imma*, *Ima2*, *Pnma*, *Pbcm*, and *Pmc2₁-I* states for our chosen chemical arrangement adopting such G-type AFM spin order. Out of these five states, the antipolar *Pnma* and polar *Ima2* phases are the two lowest-in-energy states in $\text{Ca}_2\text{FeAlO}_5$, with *Ima2* being the lowest one (which is consistent with some measurements [18,19]) but by only a minute amount of 1.35 meV per formula unit (of nine atoms). It is also interesting to realize that experiments observed the *Ima2* symmetry for the ground state of $\text{Ca}_2\text{Fe}_2\text{O}_5$ [31] versus the *Pnma* symmetry for the ground state of $\text{Ca}_2\text{Al}_2\text{O}_5$ [32]. This explains why *Ima2* and *Pnma* phases are close to each other in energy in the $\text{Ca}_2\text{FeAlO}_5$ solid solutions. Note too that the polar *Pmc2₁-I* state is also rather close in energy to *Ima2*, since it has an energy being only about 4 meV per formula unit higher than that of *Ima2*.

Moreover, Table I indicates that the electrical polarization of the polar *Ima2* state lies along along the \mathbf{b} axis and has a P_0 magnitude of $2.14 \mu\text{C}/\text{cm}^2$, respectively. Note that this value is about one order of magnitude smaller than that of the prototypical proper ferroelectric BaTiO_3 ($30 \mu\text{C}/\text{cm}^2$) [33] while it is between one and two orders of magnitude larger than that of some improper ferroelectrics [34–37]. Interestingly, the *Pmc2₁-I* phase also possesses a polarization along the \mathbf{b} axis but with a magnitude that is about $P_0/2$ (i.e., roughly half of that of *Ima2*), while *Imma*, *Pnma*, and *Pbcm* have a vanishing overall polarization. All these facts can be understood by the following rules: (1) (001) layers having their oxygen tetrahedra of types “1” and “2” tilting in a counterclockwise (respectively, clockwise) manner generate electric dipoles pointing along $+\mathbf{b}$ (respectively, $-\mathbf{b}$) in such layers, as a result of the displacement of the Al^{3+} ion away from the center of oxygen tetrahedra and along the $+\mathbf{b}$ (respectively, $-\mathbf{b}$) axis; (2) (001) layers having their oxygen tetrahedra of types “3” and “4” tilting in a counterclockwise (respectively, clockwise) manner possess electric dipoles lying along $-\mathbf{b}$ (respectively, $+\mathbf{b}$) in these layers, as a result of Al^{3+} ions moving in an opposite manner with respect to the previous case (1) [see schematization in Fig. 1(b)]; and (3) an overall electric dipole cannot exist in (001) layers that do not exhibit tilting of its oxygen tetrahedra or possess an equal number of “p” and “m” oxygen tetrahedra tiltings among tetrahedra of types 1 and 2 (or among tetrahedra of types 3

TABLE I. The lattice constants, a, b, c ; the formula unit volume, V ; the number of formula units in crystal cell, Z ; total energy, E ; polarization, \mathbf{P} ; direction of the dominant G-type AFM vector, \mathbf{L} ; and direction and magnitude of the weak magnetization, \mathbf{M} , of $\text{Ca}_2\text{FeAlO}_5$ in various states including ones with long periods. The zero of energy corresponds to the internal energy of the $Ima2$ state, and P_0 is the magnitude of the polarization in this $Ima2$ state.

Space group	$Ima2$	$Pnma$	$Pmc2_1-I$	$Pbcm$	$Imma$	$Pmc2_1-II$	$Pnc2$	$Pmc2_1-III$
Pattern	mm/pp	pp/pp	mm/mp	mp/mp	a	b	c	d
a (Å)	5.659	5.648	11.318	11.322	5.600	5.651	5.660	5.652
b (Å)	5.395	5.399	5.397	5.398	5.508	5.399	5.401	5.404
c (Å)	14.497	14.517	14.508	14.508	14.419	29.027	43.472	43.510
V (Å ³ /f.u.)	110.65	110.68	110.77	110.83	111.18	110.71	110.73	110.75
Z	4	4	8	8	4	8	12	12
E (meV/f.u.)	0.00	1.35	4.01	7.02	357.7	0.72	0.18	-0.09
P ($\mu\text{C}/\text{cm}^2$)	$2.14(P_0)$	0	$1.21(\simeq P_0/2)$	0	0	$1.17(\simeq P_0/2)$	$0.73(\simeq P_0/3)$	$0.78(\simeq P_0/3)$
axis of \mathbf{P}	b		b			b	b	b
axis of \mathbf{L}	a	a	c	c	a	a	a	a
axis of \mathbf{M}	$-c$	$-c$	a	a	$-c$	$-c$	$-c$	$-c$
M ($10^{-3}\mu_B/\text{f.u.}$)	4.93	6.23	4.90	4.31	10.5	6.26	4.99	4.82

^aNo tetrahedral tiltings in this state.

^bmm/pp/pp/pp.

^cmm/pp/pp/mm/mm/pp.

^dmm/pp/pp/pp/pp/pp.

and 4). Rule (3) naturally explains why the $Imma$ (which has no oxygen tetrahedra tiltings) and $Pbcm$ (which exhibits the mp/mp pattern) structures of brownmillerites do not possess any polarization. Furthermore, the combination of rules (1) and (2) indicates that any two neighboring (001) oxygen tetrahedra layers have exactly opposite overall electric dipoles in the $Pnma$ state (that has a “pp/pp” pattern), therefore annihilating its macroscopic polarization while producing an antipolar/antiferroelectric state (that may be of interest for energy storage [38–40]). Interestingly, rules 1 and 2 also provide a straightforward explanation of why $Pmc2_1-I$ has a polarization being roughly half that of $Ima2$: this is because only half of the (001) layers of the $Pmc2_1-I$ state generate an overall electric dipole because of its mm/mp pattern while all the (001) layers of $Imma$ contribute to the formation of a polarization, as a result of its mm/pp pattern.

Strikingly, rules (1)–(3) can be also used to design brownmillerites with a preselected magnitude of the polarization. As a matter of fact, one “just” has to construct structures having different tilting patterns for oxygen tetrahedra of types “1”, “2”, “3”, and “4”. For instance, Fig. 2 schematizes the following novel patterns: (i) mm/pp/pp/pp, which gives rise to a phase of $Pmc2_1$ symmetry containing 72 atoms per unit cell and that we denote as $Pmc2_1-II$; (ii) mm/pp/pp/mm/mm/pp, which induces a $Pnc2$ state having 108 atoms in its unit cell; and (iii) mm/pp/pp/pp/pp/pp, which yields another phase of $Pmc2_1$ symmetry but with 108 atoms per unit cell and that we coined $Pmc2_1-III$. The application of rules (1) and (2) to these three states predicts that they should all have a polarization lying along the $+\mathbf{b}$ axis but of magnitude equal to $P_0/2$ for $Pmc2_1-II$ versus $P_0/3$ for both $Pnc2$ and $Pmc2_1-III$. Additional first-principles calculations we performed for these three long-period phases, and for which results are also reported in Table I, do confirm that such predictions are rather accurate, which also demonstrates the power of rules (1)–(3) for a material-by-design strategy. Table I also reports the computed total energy of all these phases and reveals that

our *ab initio* simulations predict that $Pmc2_1-III$ is likely the ground state of $\text{Ca}_2\text{FeAlO}_5$ brownmillerites, since it has an energy being about 0.09 meV lower than that of the simpler $Ima2$ state. In fact, Table I indicates that various phases have similar energy (e.g., within about 1 meV per f.u.), such as $Ima2$, $Pnma$, $Pmc2_1-II$, $Pnc2$, and $Pmc2_1-III$, therefore pointing to the possibility of finding unusual characteristics in this system (such as nonergodicity or x rays changing with time as reported for EuTiO_3 [41]). The origin of such similarity in energy can be traced back to some phonon branches being soft and flat as a result of easily and “energetically equally” tilting the oxygen tetrahedra within different patterns, as shown in Fig. S2 of the Supplemental Material [9].

Let us now focus on the magnetic properties of all aforementioned phases. Such properties are reported for the “simple” $Imma$, $Ima2$, $Pnma$, $Pbcm$, and $Pmc2_1-I$ phases as well as the longer-period $Pmc2_1-II$, $Pnc2$, and $Pmc2_1-III$ states in Table I. Interestingly, all these states possess a weak magnetization, \mathbf{M} , that arises from the spin-orbit-induced canting of their antiferromagnetic vector, \mathbf{L} . The coexistence of

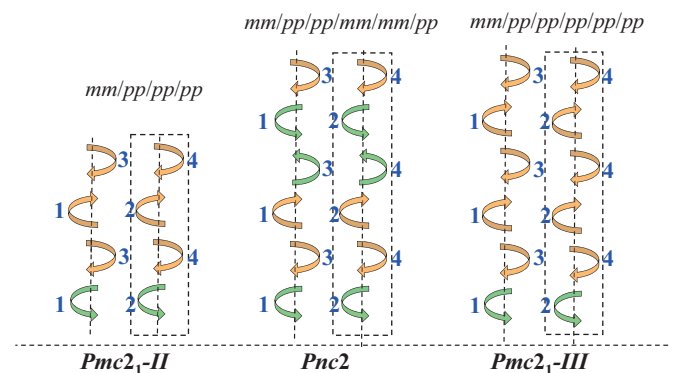


FIG. 2. Other polar phases with longer periods, and their tilting patterns, in brownmillerites. The tetrahedra of types “1”, “2”, “3”, and “4” are indicated there too.

this weak magnetization with polarization in $Ima2$, $Pmc2_1-I$, $Pmc2_1-II$, $Pnc2$, and $Pmc2_1-III$ therefore makes them multiferroic and highly desirable for some potential applications, which further emphasizes the importance of brownmillerite oxides. One can also notice from Table I that two different magnetic classes exist depending on the orientation of \mathbf{L} and \mathbf{M} : Class 1 gathers the paraelectric $Imma$ and $Pnma$ states, as well as the polar $Ima2$, $Pmc2_1-II$, $Pnc2$, and $Pmc2_1-III$ phases, that all have an easy axis for the G-type antiferromagnetic vector being along the \mathbf{a} axis and a resulting magnetization lying along the $-\mathbf{c}$ axis. Class 2 contains the paraelectric $Pbcm$ state and the polar $Pmc2_1-I$ phase, for which \mathbf{L} is along the \mathbf{c} axis and \mathbf{M} is along the \mathbf{a} axis. Interestingly, it appears that a correlation between oxygen tetrahedra tiltings and the magnetic class exists for the phases presently investigated: an equal number of “p” and “m” oxygen tetrahedra tiltings among tetrahedra of types 1 and 2 (and/or among tetrahedra of types 3 and 4) within a given (001) layer generates phases that belong to class 2. Otherwise, the structure belongs to class 1. Note that all the states forming class 1 have similar magnitude of the magnetization (namely, about 5–7 $m\mu_B/f.u.$), at the sole exception of $Imma$ for which the magnitude of the magnetization is about 50% bigger. Similarly, the $Pbcm$ and $Pmc2_1-I$ states spanning class 2 have magnetization of the order of 4–5 $m\mu_B/f.u.$

Interestingly, the existence of these two different classes hints towards possible striking magnetoelectric effects, such as, e.g., to rotate both the G-type AFM vector and magnetization by 90° if the application of an electric field along the \mathbf{b} axis to the $Pmc2_1-I$ state (belonging to class 2) allows the polarization to increase from $P_0/2$ to P_0 such as to induce a transition to $Ima2$ (that belongs to class 1). Let us also point out that some of the investigated states also naturally possess “usual” magnetoelectricity within the same class (i.e., without having to undergo a transition between the two aforementioned classes). For instance, the magnetic space group of the polar $Ima2$ state is $Imd'2'$ because of the orientation of its G-type antiferromagnetic vector and weak magnetization (associated with class 1). Consequently, its magnetoelectric tensor should only admit two nonzero and different components, which are α_{yz} and α_{zy} . To determine the value of α_{yz} , we applied a magnetic field along the c axis and computed the Berry-phase polarization along the b axis as a function of the magnitude of the magnetic field. Similarly, extracting α_{zy} consisted in applying a magnetic field along the b axis and obtaining the c -component polarization as a function of the magnitude of the magnetic field. As shown in Fig. 3, these two functions are linear, which allows us to compute their slopes and thus to predict an α_{zy} being equal to $-3.8 \times 10^{-7} \text{ C}/(\text{T m}^2)$ and α_{yz} being about $1.1 \times 10^{-7} \text{ C}/(\text{T m}^2)$. These values have nearly the same magnitude as the linear magnetoelectric coefficients of known transition-metal multiferroics, such as BiFeO_3 [42], Cr_2O_3 [29], LiNiPO_4 [29], and $\text{Co}_3\text{B}_7\text{O}_{13}\text{Br}$ [43]. Note that the large number of atoms in the unit cell of the other phases shown in Figs. 1 and 2 prevented us from computing their magnetoelectric tensor, while it is possible that some of them have an even higher magnitude of magnetoelectricity. We also obtain the magnetic transition temperature using the mean-field formula $T_N = (E_{\text{FM}} - E_{\text{AFM-G}})/6k_B$, where E_{FM} and $E_{\text{AFM-G}}$ are the DFT energy per

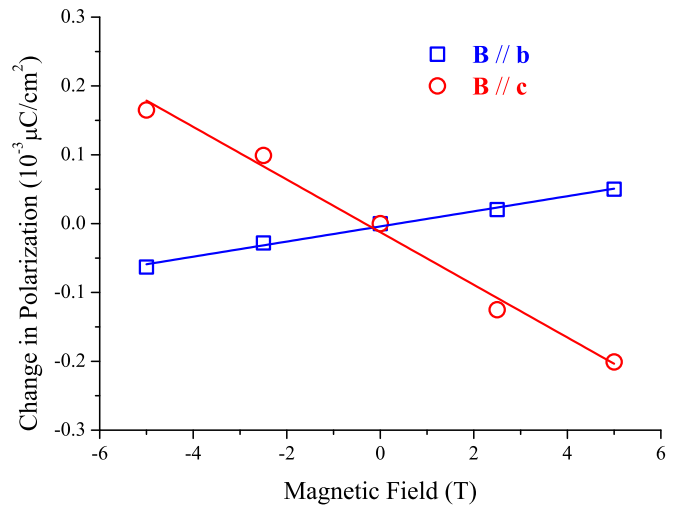


FIG. 3. Dependency of the change in polarization of (i) the b component of the polarization as a function of the magnitude of a magnetic field applied along the c axis (red data) and (ii) the c component of the polarization as a function of a magnetic field applied along the b axis in the $Ima2$ state of $\text{Ca}_2\text{FeAlO}_5$ (blue data). Solid lines show the fittings of these first-principles data by straight lines, which result in predicting the linear magnetoelectric coefficients to be $\alpha_{yz} = 1.1 \times 10^{-7} \text{ C}/(\text{T m}^2)$ and $\alpha_{zy} = -3.8 \times 10^{-7} \text{ C}/(\text{T m}^2)$.

formula unit of the ferromagnetic and G-type antiferromagnetic states for the $Ima2$ phase of $\text{Ca}_2\text{FeAlO}_5$, respectively, and k_B is the Boltzmann constant. We numerically found such transition to be about 429 K, which is consistent with the measured value of 350 K [44], especially when recalling that mean-field approaches neglect spin fluctuations and thus have the tendency to overestimate magnetic transition temperatures. Consequently, $\text{Ca}_2\text{FeAlO}_5$ should be multiferroic near room temperature with a likely sizable magnetoelectricity, since linear magnetoelectricity typically and significantly increases when heating the system from 0 K to the Néel temperature [45–47].

In summary, first-principles calculations conducted on the classical brownmillerite $\text{Ca}_2\text{FeAlO}_5$ revealed the crucial role of oxygen tetrahedral tiltings on the diversity of energetically close phases (including presently discovered long-period states) having rather different structural, electrical, magnetic, and magnetoelectric properties. More precisely, we report the findings that brownmillerite oxides (1) are even more diverse and richer than currently thought; (2) can exhibit a quantification of their electrical polarization via the tuning of the oxygen tetrahedral tilting pattern; (3) possess a rotating easy magnetic axis (of the antiferromagnetic vector) and a magnetization direction changing when going from one phase to another, via the application of an electric field; and (4) even result in the creation of room-temperature multiferroic phases with significant magnetoelectric responses. In fact, we numerically found (see Table SV of the Supplemental Material [9]) that such energetically close states exist in several other materials, such as $\text{Ca}_2\text{Fe}_2\text{O}_5$, $\text{Sr}_2\text{Fe}_2\text{O}_5$, and $\text{Ca}_2\text{Al}_2\text{O}_5$, which therefore make them general to brownmillerites. We thus hope that the present study will open a new avenue towards the design of functional materials and the systematic control of their properties.

Y.Y. and L.B. acknowledge support from ONR Grant No. N00014-17-1-2818. Y.Y. and H.T. also acknowledge the State Key Program for Basic Research of China (Contract No. 2015CB921203) and NSFC (Contract No. 11874207). H.T. also acknowledges the support of the China Postdoctoral

Science Foundation (Grant No. 2018M642205) and the Jiangsu Planned Projects for Postdoctoral Research Funds (Grant No. 2019K249). The High Performance Computing Center of Nanjing University is also acknowledged for use of its blade cluster system.

- [1] T. R. Paudel, S. S. Jaswal, and E. Y. Tsymlal, *Phys. Rev. B* **85**, 104409 (2012).
- [2] N. Lu, P. Zhang, Q. Zhang, R. Qiao, Q. He, H.-B. Li, Y. Wang, J. Guo, D. Zhang, Z. Duan *et al.*, *Nature (London)* **546**, 124 (2017).
- [3] H.-B. Li, N. Lu, Q. Zhang, Y. Wang, D. Feng, T. Chen, S. Yang, Z. Duan, Z. Li, Y. Shi *et al.*, *Nat. Commun.* **8**, 2156 (2017).
- [4] Y. Yang, C. Ma, M. Liu, H. J. Zhao, Y. Lin, C. Chen, and L. Bellaiche, *Phys. Rev. B* **95**, 165132 (2017).
- [5] H. Jeon, Z. Bi, W. S. Choi, M. F. Chisholm, C. A. Bridges, M. P. Paranthaman, and H. N. Lee, *Adv. Mater.* **25**, 6459 (2013).
- [6] A. Khare, D. Shin, T. S. Yoo, M. Kim, T. D. Kang, J. Lee, S. Roh, I.-H. Jung, J. Hwang, S. W. Kim, T. W. Noh, H. Ohta, and W. S. Choi, *Adv. Mater.* **29**, 1606566 (2017).
- [7] J. E. Auckett, A. J. Studer, E. Pellegrini, J. Ollivier, M. R. Johnson, H. Schober, W. Miiller, and C. D. Ling, *Chem. Mater.* **25**, 3080 (2013).
- [8] J. Young, E. J. Moon, D. Mukherjee, G. Stone, V. Gopalan, N. Alem, S. J. May, and J. M. Rondinelli, *J. Am. Chem. Soc.* **139**, 2833 (2017).
- [9] See Supplemental Material at <http://link.aps.org/supplemental/10.1103/PhysRevB.100.220103> for details about the methods used as well as additional information.
- [10] P. Battle, T. Gibb, and P. Lightfoot, *J. Solid State Chem.* **76**, 334 (1988).
- [11] A. Abakumov, A. Alekseeva, M. Rozova, E. Antipov, O. Lebedev, and G. Van Tendeloo, *J. Solid State Chem.* **174**, 319 (2003).
- [12] C. Didier, J. Claridge, and M. Rosseinsky, *J. Solid State Chem.* **218**, 38 (2014).
- [13] J. Zhang, H. Zheng, C. D. Malliakas, J. M. Allred, Y. Ren, Q. Li, T.-H. Han, and J. Mitchell, *Chem. Mater.* **26**, 7172 (2014).
- [14] F. Ramezanipour, J. E. Greedan, A. P. Grosvenor, J. F. Britten, L. M. Cranswick, and V. O. Garlea, *Chem. Mater.* **22**, 6008 (2010).
- [15] E. Sullivan, J. Hadermann, and C. Greaves, *J. Solid State Chem.* **184**, 649 (2011).
- [16] A. Muñoz, C. de la Calle, J. A. Alonso, P. M. Botta, V. Pardo, D. Baldomir, and J. Rivas, *Phys. Rev. B* **78**, 054404 (2008).
- [17] A. Colville and S. Geller, *Acta Crystallogr., Sect. B* **27**, 2311 (1971).
- [18] R. Grant, S. Geller, H. Wiedersich, U. Gonser, and L. Fullmer, *J. Appl. Phys.* **39**, 1122 (1968).
- [19] G. Sharma, D. Kumar, S. Tyagi, V. R. Reddy, R. Rawat, A. K. Sinha, N. P. Lalla, and V. Sathe, *J. Alloys Compd.* **732**, 358 (2018).
- [20] W. Kohn and L. J. Sham, *Phys. Rev.* **140**, A1133 (1965).
- [21] G. Kresse and J. Furthmüller, *Phys. Rev. B* **54**, 11169 (1996).
- [22] J. P. Perdew, K. Burke, and M. Ernzerhof, *Phys. Rev. Lett.* **77**, 3865 (1996).
- [23] Y. Yang, W. Ren, M. Stengel, X. H. Yan, and L. Bellaiche, *Phys. Rev. Lett.* **109**, 057602 (2012).
- [24] R. D. King-Smith and D. Vanderbilt, *Phys. Rev. B* **47**, 1651 (1993).
- [25] R. Resta, M. Posternak, and A. Baldereschi, *Phys. Rev. Lett.* **70**, 1010 (1993).
- [26] H. T. Stokes and D. M. Hatch, *J. Appl. Crystallogr.* **38**, 237 (2005).
- [27] M. Ye and D. Vanderbilt, *Phys. Rev. B* **89**, 064301 (2014).
- [28] M. Ye and D. Vanderbilt, *Phys. Rev. B* **92**, 035107 (2015).
- [29] E. Bousquet, N. A. Spaldin, and K. T. Delaney, *Phys. Rev. Lett.* **106**, 107202 (2011).
- [30] H. Tian, X.-Y. Kuang, A.-J. Mao, Y. Yang, H. Xiang, C. Xu, S. O. Sayedaghaee, J. Íñiguez, and L. Bellaiche, *Phys. Rev. Mater.* **2**, 084402 (2018).
- [31] I. Kagomiya, Y. Hirota, K.-i. Kakimoto, K. Fujii, M. Shiraiwa, M. Yashima, A. Fuwa, and S. Nakamura, *Phys. Chem. Chem. Phys.* **19**, 31194 (2017).
- [32] V. Kahlenberg, R. X. Fischer, and C. S. Shaw, *Am. Mineral.* **85**, 1061 (2000).
- [33] G. Kwei, A. Lawson, S. Billinge, and S. Cheong, *J. Phys. Chem.* **97**, 2368 (1993).
- [34] C. Xu, Y. Li, B. Xu, J. Íñiguez, W. Duan, and L. Bellaiche, *Adv. Funct. Mater.* **27**, 1604513 (2017).
- [35] T. Kimura, T. Goto, H. Shintani, K. Ishizaka, T.-h. Arima, and Y. Tokura, *Nature (London)* **426**, 55 (2003).
- [36] S. Sawada, Y. Shiroishi, A. Yamamoto, M. Takashige, and M. Matsuo, *J. Phys. Soc. Jpn.* **43**, 2099 (1977).
- [37] K. Aiki, K. Hukuda, and O. Matumura, *J. Phys. Soc. Jpn.* **26**, 1064 (1969).
- [38] B. Xu, J. Íñiguez, and L. Bellaiche, *Nat. Commun.* **8**, 15682 (2017).
- [39] L. Zhao, Q. Liu, J. Gao, S. Zhang, and J.-F. Li, *Adv. Mater.* **29**, 1701824 (2017).
- [40] X. Hao, J. Zhai, and X. Yao, *J. Am. Ceram. Soc.* **92**, 1133 (2009).
- [41] J.-W. Kim, P. Thompson, S. Brown, P. S. Normile, J. A. Schlueter, A. Shkabko, A. Weidenkaff, and P. J. Ryan, *Phys. Rev. Lett.* **110**, 027201 (2013).
- [42] I. A. Kornev, S. Lisenkov, R. Haumont, B. Dkhil, and L. Bellaiche, *Phys. Rev. Lett.* **99**, 227602 (2007).
- [43] E. Bousquet and N. Spaldin, *Phys. Rev. Lett.* **107**, 197603 (2011).
- [44] S. Geller, R. Grant, and A. Colville, *J. Phys. Chem. Solids* **34**, 107 (1973).
- [45] S. Prosandeev, I. A. Kornev, and L. Bellaiche, *Phys. Rev. B* **83**, 020102(R) (2011).
- [46] M. Mostovoy, A. Scaramucci, N. A. Spaldin, and K. T. Delaney, *Phys. Rev. Lett.* **105**, 087202 (2010).
- [47] A. Scaramucci, E. Bousquet, M. Fechner, M. Mostovoy, and N. A. Spaldin, *Phys. Rev. Lett.* **109**, 197203 (2012).